Large-eddy simulation study of upstream boundary conditions influence upon a backward-facing step flow

Jean-Luc Aider [a,b,*], Alexandra Danet [a,c]

[a] *PSA Peugeot-Citroën, Research and Innovation Department, route de Gisy, 78943 Vélizy-Villacoublay, France*
[b] *Laboratoire PMMH, ESPCI, 10, rue Vauquelin, 75231 Paris cedex 05, France*
[c] *LEGI, équipe MoST, BP 53, 38041 Grenoble cedex 09, France*

Abstract

We use Large Eddy Simulation to investigate the influence of upstream boundary conditions on the development of a backward facing step flow. The first inlet condition consists of a mean turbulent boundary layer velocity profile perturbed by a white noise. The second relies upon a precursor calculation where the development of a quasi-temporal turbulent boundary layer is simulated. In this case, the quasi-longitudinal vortices in the upstream turbulent boundary-layer trigger the destabilization of the shear layer just behind the step, resulting in a shortening of the recirculation length and an increase of the characteristic frequency associated to the Kelvin–Helmholtz vortices. The mean flow and the characteristic frequencies of pressure fluctuations are strongly dependent of the upstream flow. It demonstrates the importance of realistic boundary conditions for the simulation of complex 3D flows or for flow control simulations. ***To cite this article: J.-L. Aider, A. Danet, C. R. Mecanique 334 (2006).***
© 2006 Académie des sciences. Published by Elsevier SAS. All rights reserved.

Résumé

Étude par simulation des grandes échelles de l'influence des conditions aux limites amont sur l'écoulement derrière une marche descendante. On étudie grâce à la simulation des grandes échelles l'influence des conditions aux limites amont sur l'écoulement en aval d'une marche descendante. La première condition consiste à ajouter un bruit blanc (BB) à un profil de vitesse de couche limite turbulente. La seconde s'appuie sur un calcul précurseur (CP) où on simule le développement d'une couche limite turbulente quasi-périodique. Dans ce dernier cas, les tourbillons quasi-longitudinaux de la couche limite amont provoquent une dé-stabilisation précoce de la couche de mélange en aval de la marche. Ceci conduit à une réduction de la longueur de recirculation et à une modification des fréquences caractéristiques. La fréquence associée aux tourbillons de Kelvin–Helmholtz est nettement aug-mentée. Ces résultats soulignent l'importance des conditions aux limites amonts pour la simulation d'écoulements 3D complexes et pour les problèmes de contrôle d'écoulement. ***Pour citer cet article : J.-L. Aider, A. Danet, C. R. Mecanique 334 (2006).***
© 2006 Académie des sciences. Published by Elsevier SAS. All rights reserved.

---

* Corresponding author.
E-mail address: aider@pmmh.espci.fr (J.-L. Aider).

1. Introduction

The influence of inlet conditions, if properly defined, can be visible further downstream. The definition of the boundary conditions, especially for a spatially developing flow, is then essential but also a pretty difficult task. From the industrial point of view, it still is a challenge to perform Large Eddy Simulation (LES) computations around large and complex geometries. In automotive or train industries, for instance, engineers are interested in aeroacoustic noises generated around the vehicles. Most of the time it will be necessary to use unsteady aerodynamic flow fields, usually obtained through LES simulations, as inputs for acoustic computations. In practice the LES simulation is achieved only around the specific geometry (like an external rear view mirror) isolated from the vehicle. The problem is then to define proper spatial and temporal perturbations to add to the mean inlet condition [1] to recover a realistic upstream flow. Previous academic works considered the influence of upstream conditions on downstream evolution of a turbulent flow [2,3]. For instance, Isomoto [2] studied how the turbulence intensity imposed at the inlet of the computation domain modifies the recirculation length downstream of a backward facing step. But most of these studies focused on temporally and/or spatially averaged quantities. In this study we focus on the unsteady characteristics of the backward-facing step (bfs) flow and on their modifications when the inlet condition is changed from a random or synthetic fluctuations to a precursor domain computation.

2. Numerical domain and procedure

The governing equations are the compressible Navier–Stokes equations expressed in the conservative form. The calculations were performed with a multi-domain compressible code using Mac-Cormack finite difference numerical method. The scheme is second order accurate in time and fourth order in space. The system is filtered with an implicit spatial filter using the Favre decomposition. To close the set of equations obtained through filtering the subgrid stress tensor has to be prescribed.

The model applied in this study is based on the eddy-viscosity concept and uses the second order Structure Functions of the resolved velocity field where the turbulent viscosity introduced ν_t is written:

$$\nu_t(x,t) = C_{sf}\Delta\sqrt{\overline{F}_{2,\Delta}(x,t)}, \quad C_{sf} = 0.105 C_K^{-3/2} \tag{1}$$

This approach has been proposed by [4] and we use an extension of this model, the Filtered Structure Function model developed by [5,6] in its four points version. The objective of this extension is to reduce the weight of the large scale information when determining the structure function. This is achieved by filtering the velocity field before computing its structure function.

The parameters defining the main numerical domain used for the computations are represented on the Fig. 1. The three coordinates x, y, z, represent respectively the longitudinal, cross-stream and transverse directions. The origin of the longitudinal axis $x = 0$ is taken at the edge of the step. All quantities are normalized by the step height h and the free-stream longitudinal velocity U_0 imposed at the inlet of the domain. The computational domain consists of
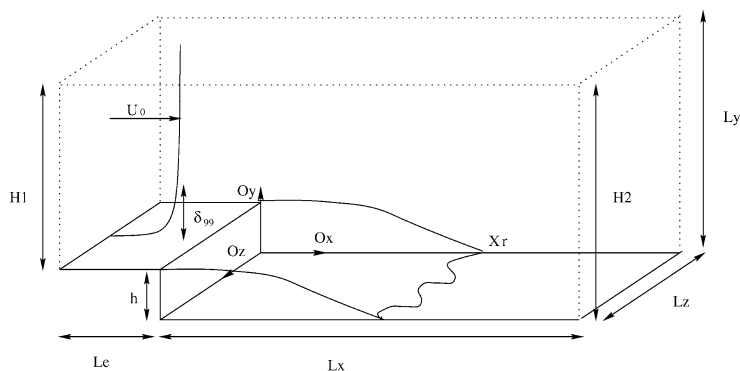

Fig. 1. Description of the main computational domain.

Fig. 1. Description du domaine principal de calcul.

an inlet section $L_i = 2.5h$ prior to the sudden expansion which extends over $L_x = 18h$. The dimensions in the other directions are respectively $(L_y, L_z) = (6h, 4h)$. The expansion ratio $Er = H_2/H_1$, i.e. the ratio between the domain height downstream and upstream of the step is 1.2. All these dimensions and the corresponding Reynolds number based on the step height ($Re_h = 5100$) are the same as in the DNS of Le et al. [7]. The only difference is the condition applied to the upper boundary, which is an outflow condition in our case while it is a no-stress wall in the DNS of Le et al. The Mach number is $Ma = 0.3$ so that the flow is only weakly compressible (no compressible effects) and our results can be compared to other incompressible experiments or simulations [7,8]. The boundary layer thickness at the inlet of the computational domain is $\delta_{99} \approx 1.2h$. We use a structured mesh, with a uniform grid in the transverse direction. In the vertical and longitudinal directions the mesh is refined in the strong shear flow regions, i.e. close to the walls and downstream of the step edge.

3. Upstream conditions

3.1. White noise (WN)

The first inlet condition used in this study consists of a mean turbulent profile perturbed by a white noise. The longitudinal mean velocity is fitted to the profile of the Direct Numerical Simulation of a turbulent boundary layer computed by [9] with a Reynolds number $Re_\theta = 670$ ($Re_\delta^* = 1000$). Here θ is the momentum thickness and $\delta_{99} = 6.1\delta^*$. The vertical and spanwise components of the mean velocity are set to zero. At every time step random fluctuations are superimposed on the inflow profile. The maximum intensity of the noise is set to $1.5U_0$ and is applied in the region where $y \leqslant \delta_{99}$. As noticed by Fureby [10] the results are insensitive to the level of prescribed fluctuations. In fact, the lack of spatial and temporal correlations leads to a sharp drop in intensity in the few nodes following the inlet. Thus we observe a turbulent longitudinal velocity profile, without any structures and associated energy, close to the separation region as witnessed on the contours of longitudinal velocity in a X plane just upstream of the step edge (Fig. 2(a)).

3.2. Precursor simulation (PS)

The second method used to generate time-dependent turbulent inflow data is the one proposed by Lund et al. [11]. It consists of an auxiliary simulation which generates its own inflow conditions through a sequence of operations where the velocity field at a downstream station is re-scaled and re-introduced at the inlet of the precursor domain. This method produces a realistic turbulent boundary layer leading to statistics that are in good agreement with target profiles previously presented. A selected vertical plane at the exit of this precursor domain is then extracted, stored and re-introduced afterwards as inflow conditions for the step domain (Fig. 3). The computational domain of the precursor required about 350 000 grid points for the following dimensions $(L_x, L_y, L_z) = (10h, 5h, 4h)$ and a grid resolution corresponding to the main domain. The recycling position X_{recy} where the data are stored was set to $8h$.
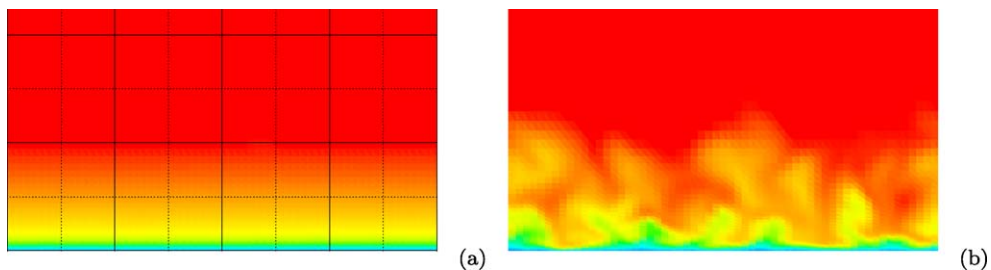

(a)　(b)

Fig. 2. Visualization of the instantaneous longitudinal adimensionalized velocity field in the cross-section just upstream of step edge: (a) WN, (b) PS.

Fig. 2. Visualisation du champ de vitesse longitudinale juste en amont de la marche : (a) Bruit Blanc (BB) ; (b) Calcul Précurseur (CP).
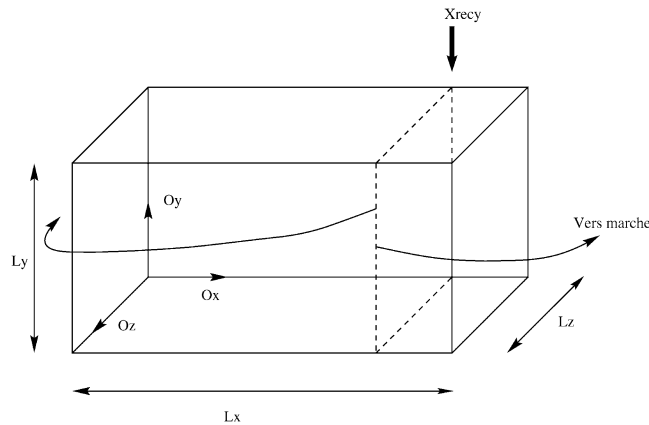
Fig. 3. Description of the precursor domain. The plane $X_{\mathrm{recy}} = 8h$ is used as inlet boundary for the main domain and for the precursor domain.

Fig. 3. Description du domaine précurseur. Le plan $X_{\mathrm{recy}} = 8h$ sert à initier le calcul précurseur et le domaine aval.

4. Modification of the backward-facing step flow by the upstream boundary conditions

On Fig. 4 we show a 3D view of the instantaneous coherent structures for the two simulations. The qualitative differences between the two simulations are obvious: in the PS case the upstream boundary layer contains turbulent structures and the shear layer downstream of the step becomes more quickly unstable compared to the WN case. As expected the destabilization of the shear layer has consequences on the mean flow (averaged in time and space). We find a mean recirculation length $X_r = 5.80h$ for the WN simulation and $X_r = 5.29h$ for the PS. The recirculation length is clearly decreased in the PS case, i.e. when the shear layer is destabilized by the incident turbulent structures (Fig. 5). This is to be compared with the numerical results of Le et al. [7] ($X_r = 6.28h$) and the experimental measurements of Jovic and Driver [8] ($X_r \approx 6h$). In both cases, the recirculation length is shorter than in the previous works which can be explained by the different upper boundary conditions: we observed, in a test case, an increase of the recirculation length when the upper boundary is changed from outflow to sliding wall.

If the averaged quantities are often discussed in the studies dealing with the backward-facing step flow, it is more difficult to find references dealing with unsteady behavior of the flow. Our point of view is that it is essential to check if we get the right frequencies if we want to use the simulation for flow control 'numerical experiments'. In this section we focus on the modification of the characteristic frequencies of pressure fluctuations obtained in different probes located downstream of the step (Fig. 6), in the shear layer and close to the lower wall downstream of the step.
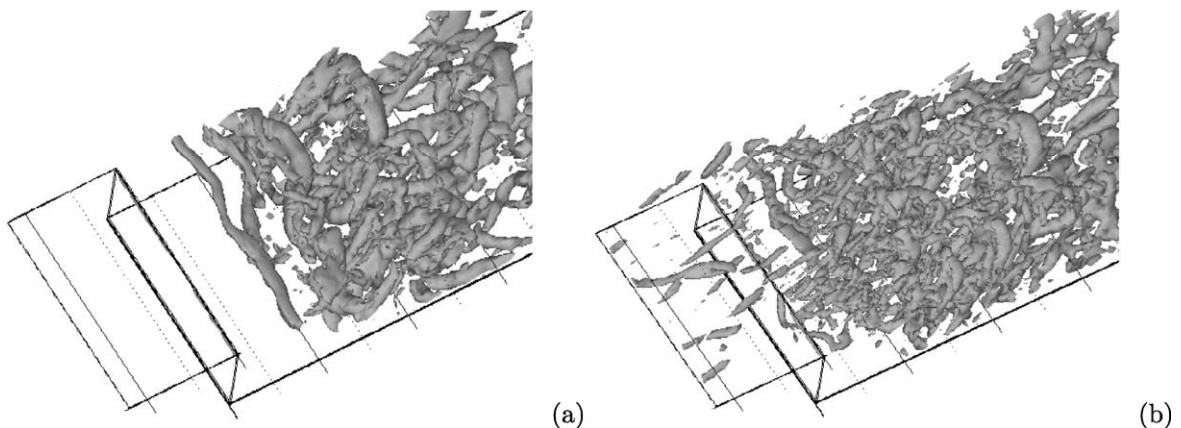

Fig. 4. Visualization of the instantaneous field of coherent structures using the Q criterium ($Q = 0.5U_0^2/h$): (a) WN case, (b) PS case.

Fig. 4. Visualisation des structures cohérentes à l'aide du critère Q ($Q = 0.5U_0^2/h$) : (a) Bruit Blanc, (b) Calcul Précurseur.
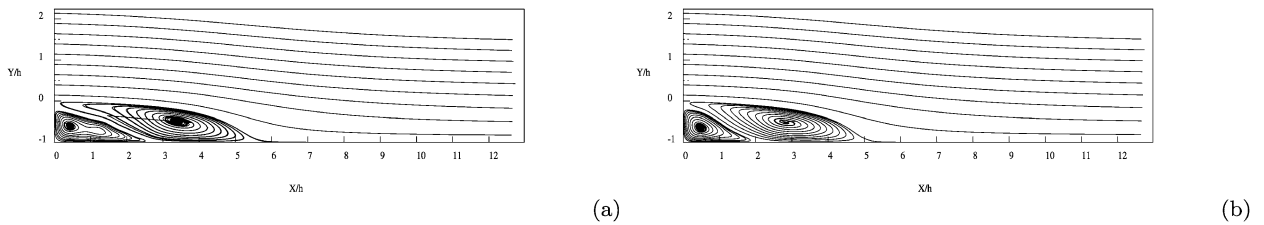
Fig. 5. Contours of stream-function for the two simulations (averaged over time and space): (a) WN case, (b) PS case.

Fig. 5. Lignes de courant pour les deux simulations (moyennées en temps et en espace) : (a) BB, (b) CP.
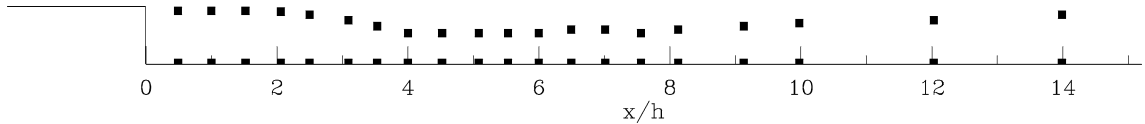

Fig. 6. Localization of the pressure probes downstream of the step (WN and PS) along the shear layer, at the vertical position where the longitudinal turbulence intensity is maximum, and close to the wall.

Fig. 6. Positionnement des sondes de pression en aval de la marche, dans la région de couche de mélange, où les intensités turbulentes sont les plus fortes, et près de la paroi.
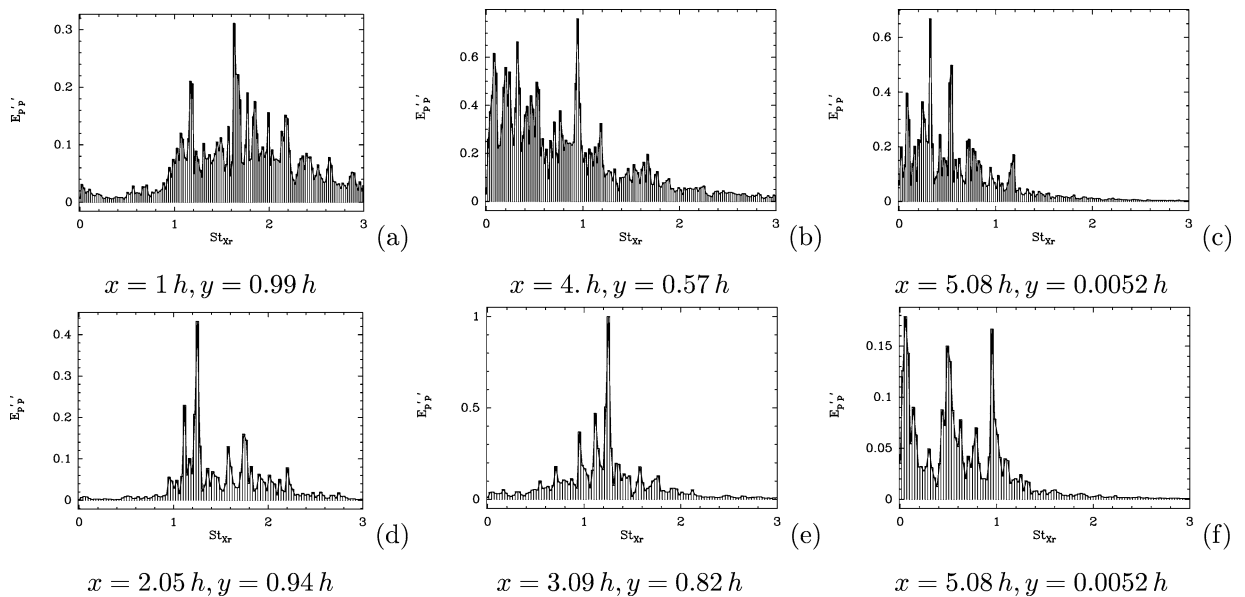

Fig. 7. Examples of spectra of local pressure fluctuations in three positions in the domain downstream of the step in the PS ((a), (b), (c)) and WN cases ((d), (e), (f)): (a), (d) in the shear layer downstream of the step, (b), (e) further downstream in the shear layer, (c), (f) in the reattachment region. To make the comparison easier, we do not use the same probes in the figures (a) and (d) as well as in the figures (b) and (e).

Fig. 7. Spectres des fluctuations de pression en trois positions en aval de la marche : cas CP ((a), (b), (c)) et cas BB ((d), (e), (f)) : (a), (d) dans la couche de mélange en aval de la marche, (b), (e) un peu plus en aval dans la couche de mélange, (c), (f) au point de recollement. Pour faciliter les comparaisons nous n'utilisons pas les mêmes sondes pour les figures (a) et (d) ainsi que pour les figures (b) et (e).

We use a Strouhal number defined as the frequency adimensionalized by the averaged recirculation length, X_r, and the freestream velocity U_0: $St = f X_r / U_0$. As the flow is homogeneous in the spanwise direction, the spectra are averaged along this direction to ensure statistical convergence. We show on Fig. 7 a typical example of the pressure spectra obtained with different pressure probes in the PS case (Figs. 7(a)–(c)) and the WN case (Figs. 7(d)–(f)). The spectra are adimensionalized by the amplitude of the highest peak obtained for each time series to help the comparison. The first probe is located in the shear layer downstream of the step, the second is further downstream, in the mixing layer, while the third probe is in the reattachment region. The location of the two first probes is slightly different in

the PS case than in the WN case to compare the frequencies at the longitudinal location where the amplitude of the peaks is the highest. This is also a first evidence of the effect of the upstream boundary conditions: the longitudinal evolution of the characteristic frequencies is different in the two cases.

The frequencies are well defined and the modification of the spectra between the three longitudinal positions is important. If we consider the overall spatial evolution of all the spectra (which cannot be shown in this paper), one can find the main characteristic frequencies of the major phenomena, with dominant high frequencies close to the edge and increasing low frequencies band further downstream.

In the shear layer, close to the edge of the step, one can see a high frequency around $St = f X_r / U_0 = 1.24$ for the WN case and $St = f X_r / U_0 = 1.63$ for the PS case (Figs. 7(a) and (d)). Considering the probes location, the dominant frequencies can be associated to the Kelvin–Helmholtz (KH) vortices in both cases. This frequency is dominant in the range $[0.5h–1.5h]$ for the PS case and in the range $[2h–4h]$ in the WN case. As expected, the incoming boundary layer has a strong influence on the shear layer instability: if we compare the real frequencies, one find $f_{PS} = 1.7 \times f_{WN}$. The destabilization of the shear layer is clearly triggered by the turbulent boundary layer. Further downstream in the shear layer, one can see the growth of lower frequencies and especially a peak around $St = 0.94$, for the PS case and the WN case, corresponding to the pairing of the KH vortices (Figs. 7(b) for the PS case and 7(f) for the WN case). This frequency is dominant in the range $[3h–4h]$ for the PS case and in the range $[4.5h–5.5h]$ in the WN case. Finally, in the reattachment region, two lower frequencies become dominant (Figs. 7(c) and 7(f)): one around $St = 0.50–0.54$, for both cases, corresponding to the oscillations of the recirculation bubble, and one peak around $St = 0.08$ for the WN case and $St = 0.34$ for the PS case corresponding to the flapping of the shear layer.

To summarize, the Precursor Simulation leads to higher frequencies than the WN case for the KH vortices and the flapping of the shear layer. On the contrary, the frequencies associated to the pairing of the KH vortices and to the oscillation of the recirculation bubble are less dependent of the upstream boundary layer. As expected with the modification of the mean flow (smaller recirculation length in the PS case), the spatial evolution of the characteristic frequencies is also different in the two cases.

We report in Table 1 the frequencies for the two simulations together with the results of other studies. For the sake of comparison, the data from the other studies are recalculated using the same definition of the Strouhal number (with X_r). Our results compare reasonably well with the one observed in the previous works, even if no one ever characterized the four frequencies. In fact, the oscillation of the recirculation bubble is the only phenomenon that has been observed in all the studies, with a mean Strouhal number $\langle St_{exp} \rangle = 0.66$ for the experiments and $\langle St \rangle_{num} = 0.53$ for the numerical simulation. Our results correspond to the average of the other numerical studies which tend to underestimate this frequency compared to the experimental results. The dispersion observed for the frequency associated with the KH vortices can be explained by the high sensitivity to upstream perturbations: it can be triggered if the shear layer is excited by a perturbation with the proper frequency [12]. The large difference between the PS and WN case is a clear proof of this mechanism which can be explained by the relatively broad frequency spectrum of

Table 1

Typical frequencies observed in experimental and numerical studies: $St = f X_r / U_0$. Data unknown: –. The upper part of the table corresponds to experimental results and the lower part correspond to numerical simulations

Tableau 1

Fréquences observées dans des études expérimentales et numériques précédentes : $St = f X_r / U_0$. La partie supérieure correspond à des donnés expérimentales et la partie inférieure à des données numériques. Données inconnues : –

Reference	Flapping	X_r oscillation	Pairing KH	KH
Eaton and Johnston (1982) [13]	0.152	0.52	–	–
Roos and Kegelman (1986) [14]	–	⩽0.68	1.1	2.2
Driver et al. (1987) [15]	0.12	0.7	–	–
Devenport and Sutton (1991) [16]	0.18	0.74	–	–
Arnal and Friedrich (1991) [17]	0.07–0.3	0.5–0.7	–	2
Silveira Neto et al. (1993) [18]	–	0.65	–	–
Le et al. (1997) [7]	–	0.38	–	–
Delcayre (1999) [19]	–	0.5	0.93	1.63
White noise	0.08	0.50	0.94	1.24
Precursor simulation	0.34	0.54	0.94	1.63

the incoming upstream turbulent boundary layer in the PS case. The same kind of explanation can be applied to the frequency associated to the flapping of the shear layer.

5. Conclusion

We have carried out an analysis of the unsteady behavior of the flow behind a backward facing step. Thanks to the analysis of pressure fluctuation time series we could identify the characteristic frequencies associated to the main instability mechanisms occurring in the shear layer and the recirculation bubble.

We were also interested in the sensitivity of the BFS flow to the modification of the upstream boundary conditions. In the case where the inlet stemmed from a precursor simulation, we show that the incoming turbulent structures significantly influence the development of the flow downstream of the step expansion. In particular the velocity streaks and quasi-longitudinal vortices trigger a rapid destabilization of the shear layer resulting in a shortening of the recirculation length. The spectra of pressure fluctuations in different positions downstream of the step edge are also strongly modified. The spectrum is much richer in the PS case and one can also observe the shifting to high frequencies of some of the characteristic frequencies, like the one associated to the KH vortices. The spatial distribution of the frequencies is also clearly modified. It illustrates the essential role of defining proper upstream conditions to correctly simulate the structure and dynamics of spatially-developing flows. It will be critical if the objective is the simulation of a flow controlled by steady or time-dependent perturbations.

References

[1] F. Mathey, D. Cokljat, J.P. Bertoglio, E. Sergent, Specification of LES inlet boundary conditions using vortex method, in: Proceedings of the 4th International Symposium on Turbulence, Heat and Mass Transfer, Antalya, Turkey, 2003.

[2] K. Isomoto, S. Honami, The effect of inlet turbulence intensity on the reattachment process over a backward-facing step, J. Fluids Eng. 111 (1989) 87–92.

[3] A. Keating, U. Piomelli, E. Balaras, H.-J. Kaltenbach, A priori and a posteriori tests of inflow conditions for large-eddy simulation, Phys. Fluids 16 (2004) 4696–4712.

[4] O. Métais, M. Lesieur, Spectral large eddy simulation of isotropic and stably stratified turbulence, J. Fluid Mech. 239 (1992) 157–194.

[5] F. Ducros, P. Comte, M. Lesieur, Large-eddy simulation of transition to turbulence in a boundary layer developing spatially over a flat plate, J. Fluid Mech. 326 (1996) 1–36.

[6] M. Lesieur, O. Métais, P. Comte, Large-Eddy Simulations of Turbulence, Cambridge Univ. Press, 2005.

[7] H. Le, P. Moin, J. Kim, Direct numerical simulation of turbulent flow over a backward-facing step, J. Fluid Mech. 330 (1997) 349–374.

[8] S. Jovic, D.M. Driver, Backward-facing step measurements at low Reynolds number, $Re_h = 5000$, NASA Tech. Mem. 108807, 1994.

[9] P.R. Spalart, Direct numerical simulation of a turbulent boundary layer up to $Re_\theta = 1410$, J. Fluid Mech. 187 (1988) 61–98.

[10] C. Fureby, Large eddy simulation of rearward-facing step flow, AIAA J. 37 (1999) 1401–1410.

[11] T. Lund, X. Wu, K.D. Squires, Generation of turbulent inflow data for spatially-developing boundary layer simulations, Phys. Fluids 140 (1998) 233–238.

[12] J. Silvestrini, Simulations des grandes échelles des zones de mélanges; application à la propulsion solide des lanceurs spatiaux, Thèse de Doctorat de l'Institut National Polytechnique de Grenoble, 1996.

[13] J.K. Eaton, J.P. Johnston, Low frequency unsteadiness of a reattaching turbulent shear layer, Turbulent Shear Flows 3 (1982) 162–170.

[14] F.W. Roos, J.K. Kegelman, Control of coherent structures in reattaching laminar and turbulent shear layer, AIAA J. 24 (1986) 1956–1963.

[15] D.M. Driver, H.L. Seegmiller, J.G. Marvin, Time-dependent behavior in a reattaching shear layer, AIAA J. 25 (7) (1987) 914–919.

[16] W.J. Devenport, E.P. Sutton, Near-wall behavior of separated and reattaching flows, AIAA J. 29 (1) (1991) 25–31.

[17] M. Arnal, R. Friedrich, Large Eddy Simulation of a turbulent flow with separation, Turbulent Shear Flows 8 (1991) 169.

[18] A. Silveira Neto, D. Grand, O. Métais, M. Lesieur, A numerical investigation of the coherent vortices in turbulence behind a backward-facing step, J. Fluid Mech. 256 (1993) 1–25.

[19] F. Delcayre, Etude par Simulation des Grandes Echelles d'un écoulement décollé : la marche descendante, Thèse de Doctorat de l'Institut National Polytechnique de Grenoble, 1999.